

Cavity-assisted Dynamical Quantum Phase Transition at Bifurcation Points

Lin Tian^{1,*}

¹*School of Natural Sciences, University of California, Merced, California 95343, USA*

Coupling a quantum many-body system to a cavity can create bifurcation points in the phase diagram, where the ground state switches between different phases. Here we study the dynamical quantum phase transition at the bifurcation points of a transverse field Ising model coupled to a cavity. We show that an infinitesimal quench of the cavity driving induces gradual evolution of the Ising model to pass across the quantum critical point and generates quasiparticles. Our calculation also shows that when the driving is slowly ramped over the bifurcation points, the adiabaticity of the evolution and the number of excitations are strongly affected by cavity-induced nonlinearity. This effect can hence be exploited to improve the fidelity of adiabatic quantum processes. Our model can be implemented with superconducting quantum circuits.

PACS numbers: 64.60.Ht, 42.50.Pq, 85.25.Cp

Introduction.—Stimulated by recent advances in manipulating atomic and solid-state quantum systems [1, 2], out-of-equilibrium many-body phenomena have been intensively studied [3–6]. One intriguing effect is the dynamical quantum phase transition of a many-body system swept across a quantum critical point. This effect was first studied using scaling laws in the seminal works of [7, 8]. It was predicted in terms of the Kibble-Zurek mechanism that the adiabaticity of a slowly-ramped system will be broken near the critical point, accompanied by the production of quasiparticles [9–12]. Various approaches to improve the adiabaticity in such dynamical processes have also been developed [13–20].

Cavity or circuit quantum electrodynamics (QED) is a powerful approach to manipulate and probe the states of quantum systems, as demonstrated in earlier experiments on single qubit [21–23]. For a cavity coupled to a large number of atoms or qubits, collective effects such as bistability and Dicke superradiance can be observed [24–29]. It was shown that multiple superconducting qubits can be coupled simultaneously to a superconducting transmission line resonator [30, 31]. Dynamical phase transition was also observed with a collection of atoms coupled to a dissipative cavity [32]. Furthermore, arrays of optical or microwave cavities can be connected to form Jaynes-Cummings lattices to emulate quantum phase transitions in cavity polaritons [33, 34]. Given these progresses, dynamical effects of many-body systems coupled to a cavity can be explored experimentally.

Here we study the dynamical quantum phase transition of a many-body system embedded in a cavity. The coupling between the many-body model and the cavity results in nonlinearity and a bistable regime in the phase diagram [26–28]. At the bifurcation points, the system switches between quantum phases of different symmetry. The switching is accompanied by finite changes in system parameters and energy, resembling a first-order phase transition [29]. How the switching across the bifurcation points occurs is an open question. We study this question with a transverse field Ising model (TFIM) [1]

coupled to a cavity. Using a time-dependent Bogoliubov method [3], we calculate the time evolution of this system undergoing sudden quench or gradual ramping of the cavity driving. We find that after an infinitesimal quench at the bifurcation points, the TFIM gradually evolves through the critical point to enter a different phase. Under slow ramping, the dynamics near the critical point and the quasiparticle excitations are strongly affected by the cavity-induced nonlinearity. Our results can be extended to general discussions of other many-body systems and other forms of cavity coupling. These findings indicate that the adiabaticity of a dynamical process can be controlled by adjusting the cavity-induced nonlinearity, which could be used to develop high-fidelity adiabatic quantum computing schemes [37–39]. The model studied here can be realized with superconducting quantum circuits. The TFIM can be emulated by arrays of superconducting qubits [29, 40–44], and the cavity by superconducting resonators.

System.—Consider a one-dimensional TFIM coupled to a cavity. The Hamiltonian of the TFIM is ($\hbar = 1$)

$$H_s = -B_x \sum_i \hat{\sigma}_{xi} - J_0 \sum_i \hat{\sigma}_{zi} \hat{\sigma}_{z(i+1)}, \quad (1)$$

where $\hat{\sigma}_{xi}$ and $\hat{\sigma}_{zi}$ are the Pauli matrices for the spin-1/2 particle at site i , B_x is a uniform transverse field, and J_0 is a ferromagnetic coupling between neighboring spins. This model is exactly solvable with the Jordan-Wigner transformation that converts the spins to fermionic particles. The ground state of this model is ferromagnetic (paramagnetic) for weak (strong) transverse field with $B_x < J_0$ ($B_x > J_0$) and a continuous quantum phase transition occurs at the critical point $B_x = J_0$ [1]. The ground state is a product state with $|G\rangle = \prod_{k>0} |G_k\rangle$ and $|G_k\rangle = (u_k + iv_k \hat{c}_k^\dagger \hat{c}_{-k}^\dagger) |0_{k,-k}\rangle$, where \hat{c}_k (\hat{c}_k^\dagger) is the annihilation (creation) operator of the fermionic particle with momentum k , $|0_{k,-k}\rangle$ is the vacuum state of the $(k, -k)$ modes, $u_k = \cos \theta_k$, and $v_k = \sin \theta_k$ as given in the Supplementary Materials [45]. In the subspace of zero or even number of excitations, the wave vectors

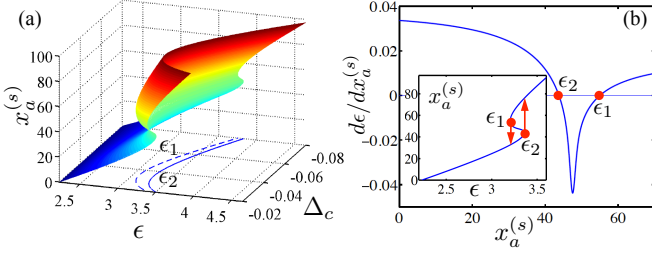


FIG. 1. (Color online) (a) The cavity displacement $x_a^{(s)}$ vs. driving amplitude ϵ and detuning Δ_c . Solid (dashed) line: the bifurcation point ϵ_2 (ϵ_1) vs. Δ_c . (b) The derivative $d\epsilon/dx_a^{(s)}$ vs. $x_a^{(s)}$ at $\Delta_c = -0.05$. Inset: $x_a^{(s)}$ vs. ϵ . Other parameters are $J_0 = 1$, $B_x = 1.95$, $g = 0.02$ and $\kappa = 0.07$, all in arbitrary units; and the TFIM has $N = 120$ sites.

are $k = \pm(2m - 1)\pi/N$ with $m = 1, \dots, N/2$ [3]. The Hamiltonian of the cavity is $H_c = H_{c0} + H_\kappa$, where

$$H_{c0} = -\Delta_c \hat{a}^\dagger \hat{a} - \epsilon(t)(\hat{a} + \hat{a}^\dagger) \quad (2)$$

describes the cavity driven by an external field $\epsilon(t)$, and H_κ describes the cavity-bath coupling. Here \hat{a} (\hat{a}^\dagger) is the annihilation (creation) operator of the cavity, Δ_c is the cavity detuning relative to the driving frequency, and the cavity is dissipative with a damping rate κ [45]. We assume the coupling between the TFIM and the cavity is

$$H_{int} = g(\hat{a} + \hat{a}^\dagger) \sum_i \hat{\sigma}_{xi}, \quad (3)$$

which can be realized in various physical systems, such as the circuit QED system [22, 23]. With this coupling, the spins shift the cavity displacement, and the cavity field modifies the transverse field on the spin particles. Other forms of coupling can also generate similar nonlinear effect as discussed in [29]. The total Hamiltonian of this system is then $H_t = H_s + H_{int} + H_c$.

Below we use a mean-field approach to treat the interaction: $(\hat{a} + \hat{a}^\dagger) \sum_i \hat{\sigma}_{xi} \approx (\hat{a} + \hat{a}^\dagger)X + x_a \sum_i \hat{\sigma}_{xi} - x_a X$, where $X = \langle \sum_i \hat{\sigma}_{xi} \rangle$ is the average of the collective spin operator $\sum_i \hat{\sigma}_{xi}$ and $x_a = \langle (\hat{a} + \hat{a}^\dagger) \rangle$ is the average of the cavity displacement. With this approximation, the total Hamiltonian can be decomposed into $H_t \approx \tilde{H}_s + \tilde{H}_c$, where \tilde{H}_s is the Hamiltonian of the TFIM with an effective transverse field $\tilde{B}_x = B_x - gx_a$ and \tilde{H}_c is for the cavity with a modified driving amplitude $\tilde{\epsilon} = \epsilon - gx_a$. The effective Hamiltonian of the TFIM (cavity) depends on the operator average of the cavity (spins). The cavity acts as a semiclassical knob that modifies the parameter in the TFIM, and at the same time, depends nonlinearly on the state of the spins. Note that in this treatment, quantum fluctuations of the cavity are neglected, which is valid at strong driving [46].

Bifurcation and stability.—The Langevin equation for the average of the cavity operator \hat{a} is [4]

$$\frac{d}{dt} \langle \hat{a} \rangle = i\Delta_c \langle \hat{a} \rangle - \frac{\kappa}{2} \langle \hat{a} \rangle + i(\epsilon - gX), \quad (4)$$

which depends on the operator average $X = \langle \sum_i \hat{\sigma}_{xi} \rangle$ of the TFIM. With this equation, the stationary cavity displacement can be derived as [45]

$$x_a^{(s)} = \frac{2\Delta_c(-\epsilon + gX^{(s)})}{\Delta_c^2 + \kappa^2/4}. \quad (5)$$

Here $X^{(s)}$ is the average of $\sum_i \hat{\sigma}_{xi}$ when the TFIM is in the ground state under an effective transverse field $\tilde{B}_x = B_x - gx_a^{(s)}$, and it has a nonlinear dependence on $x_a^{(s)}$. This nonlinearity yields a bistable regime for the cavity displacement, where there are three stationary solutions at a given driving amplitude ϵ and detuning Δ_c , as shown in Fig. 1(a). For these solutions, the stability condition is $d\epsilon/dx_a^{(s)} > 0$, as derived in the Supplemental Materials [5, 45]. In the inset of Fig. 1(b), we see that the largest and smallest solutions are stable, whereas the intermediate solution is unstable. Accordingly, $X^{(s)}$ also exhibits bistability due to its dependence on \tilde{B}_x (or $x_a^{(s)}$).

The bifurcation points satisfy $d\epsilon/dx_a^{(s)} = 0$ [red circles in Fig. 1(b)] and divide the bistable regime from regimes with only one stable solution [49]. In Fig. 1(a), the bifurcation points $\epsilon_{1,2}$ are plotted versus Δ_c , which generate a phase diagram for the cavity-coupled TFIM. The area between $\epsilon_{1,2}$ corresponds to the bistable regime where the TFIM can be in either the paramagnetic or the ferromagnetic phase, depending on the history of the evolution. At the bifurcation point ϵ_2 , the TFIM switches from the paramagnetic branch with $\tilde{B}_x > 1$ to the ferromagnetic branch with $\tilde{B}_x < 1$. Similarly, an opposite switching occurs at the bifurcation point ϵ_1 .

Quench dynamics at bifurcation points.—The switching at the bifurcation points involves finite changes in the stationary cavity displacement and phase transition in the TFIM. We study the dynamics of this switching with a time-dependent Bogoliubov method [3]. The time evolution of $x_a(t)$ is governed by Eq. (S21), which depends on the operator average $X(t)$. The dynamics of the TFIM is governed by the Schrödinger equation $i d|\psi(t)\rangle/dt = \tilde{H}_s(t)|\psi(t)\rangle$ for wave function $|\psi(t)\rangle$, where \tilde{H}_s contains a time-dependent transverse field $\tilde{B}_x(t)$ that depends on $x_a(t)$. Starting from the ground state under an initial transverse field $\tilde{B}_x(0)$, the wave function always has the form $|\psi(t)\rangle = \prod_{k>0} (U_k(t) + iV_k(t)\hat{c}_k^\dagger \hat{c}_{-k}^\dagger)|0\rangle$ with time-dependent coefficients $U_k(t)$ and $V_k(t)$ [45]. Let $U_k = \bar{U}_k e^{-i\varphi(t)}$ and $V_k = \bar{V}_k e^{-i\varphi(t)}$, with phase factor $\varphi(t) = \int_0^t dt' [-2B_x(t') + \varepsilon_k(t') \cos[2\theta_k(t')]]$ and instantaneous eigenenergy $\varepsilon_k(t)$ under the transverse field $\tilde{B}_x(t)$. We have

$$i \frac{d}{dt} \begin{bmatrix} \bar{U}_k \\ \bar{V}_k \end{bmatrix} = \begin{bmatrix} -\varepsilon_k \cos(2\theta_k) & -\varepsilon_k \sin(2\theta_k) \\ -\varepsilon_k \sin(2\theta_k) & +\varepsilon_k \cos(2\theta_k) \end{bmatrix} \begin{bmatrix} \bar{U}_k \\ \bar{V}_k \end{bmatrix}, \quad (6)$$

i.e., the evolutions in different $(k, -k)$ subspaces are independent. By solving Eqns. (S21) and (6) numerically, we obtain the dynamics of this system. Note that

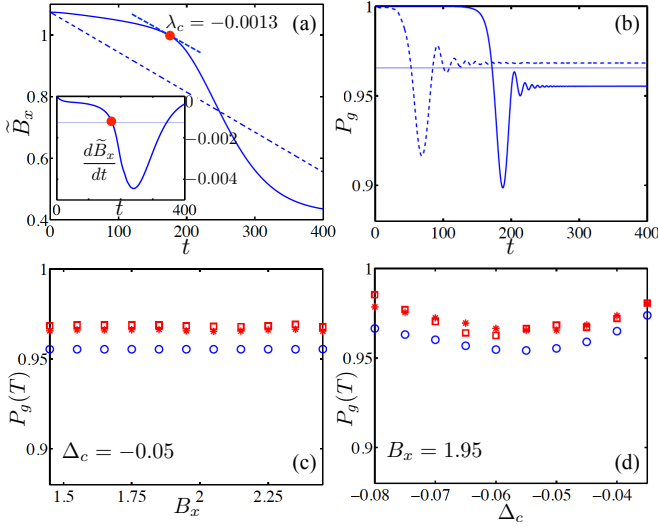


FIG. 2. (Color online) (a) The effective transverse field \tilde{B}_x and (b) the ground state probability P_g vs. time after an infinitesimal quench. Solid lines: cavity-coupled TFIM; dashed lines: linearly-ramped TFIM; thin solid line in (b): Landau-Zener formula. Inset of (a): $d\tilde{B}_x/dt$ vs. time. Red dots: the time t_c when $\tilde{B}_x = J_0$. (c) and (d) The probability $P_g(T)$ vs. B_x and Δ_c at $T = 400$. Blue circles: cavity-coupled TFIM; red squares: linearly-ramped TFIM; red stars: Landau-Zener formula. The parameters are the same as that in Fig. 1(b).

the wave function can also be expressed as $|\psi(t)\rangle = \prod_{k>0} [\alpha_k(t) + i\beta_k(t)\hat{\gamma}_k^\dagger\hat{\gamma}_{-k}^\dagger] |G_k\rangle$ in terms of the instantaneous ground state $|G_k\rangle$ and excited state $i\hat{\gamma}_k^\dagger\hat{\gamma}_{-k}^\dagger |G_k\rangle$ with probability amplitudes α_k and β_k , respectively [45].

The switching at the bifurcation points can be triggered by an infinitesimal quench of the driving amplitude. Let the system be prepared in the stationary state of an initial driving $\epsilon = \epsilon_2 - \Delta\epsilon/2$ that is right below the bifurcation point ϵ_2 . We choose $\Delta\epsilon = 0.01$ in unit of $J_0 = 1$ with $\Delta\epsilon \ll |\epsilon_2 - \epsilon_1|$. At $B_x = 1.95$ and $\Delta_c = -0.05$, $\epsilon_2 = 3.36$. The initial cavity displacement is $x_a^{(s)} = 43.78$, yielding an effective transverse field $\tilde{B}_x(0) = 1.07$. At $t = 0$, the driving is switched to $\epsilon = \epsilon_2 + \Delta\epsilon/2$, right above the bifurcation point, with $x_a^{(s)} = 75.95$. We calculate the time evolution of this system after the quench. As shown in Fig. 2(a), the effective field decreases gradually and eventually converges to the stationary value of $\tilde{B}_x = 0.43$. It reaches the critical point $\tilde{B}_x = J_0$ at $t_c \sim 160$. A small quench of the driving hence induces large changes in the system parameters and a phase transition in the TFIM. This is due to the cavity-induced nonlinearity that creates a discontinuity in the stationary solutions at the bifurcation points.

As the effective transverse field approaches the critical point, the relaxation time of the TFIM diverges as $\sim 1/(2|\tilde{B}_x - J_0|)$. When the relaxation becomes slower than the variation of the Hamiltonian, the evolution ceases to be adiabatic and quasiparticles can be excited,

as explained by the Kibble-Zurek mechanism [9–12]. In Fig. 2(b), the probability P_g for the TFIM to be in its instantaneous ground state is plotted. Far from the critical point, the TFIM evolves adiabatically with the transverse field and remains in its ground state with $P_g \approx 1$. Near $t = t_c$, P_g starts decreasing. It exhibits oscillatory behavior before reaching a stationary value of $P_g(T) = 0.955$. Hence quasiparticles are created in the TFIM, which is verified by our calculation of the excitation probability $|\beta_k(t)|^2$ of the $(k, -k)$ modes. During the entire evolution, $P_g \approx (1 - |\beta_{k=\pi/N}|^2)$, i.e., quasiparticles are mainly excited in the $(\pi/N, -\pi/N)$ modes. This effect is also observed at the bifurcation point ϵ_1 as well as in a broad range of transverse field B_x and detuning Δ_c . In Fig. 2(c) and (d), we plot the dependence of $P_g(T)$ on B_x and Δ_c at the final time of the evolution $T = 400$.

To understand this behavior, we simulate the dynamics of a simple TFIM under a linearly-ramped transverse field [3, 7, 8]. The time dependence of the transverse field is $B_x(t) = \tilde{B}_x(0) + \lambda_c t$ [dashed line in Fig. 2(a)], where $\tilde{B}_x(0)$ is the effective transverse field in the cavity-coupled TFIM at $t = 0$ and the ramping rate $\lambda_c = d\tilde{B}_x/dt|_{t=t_c}$ is the slope of $\tilde{B}_x(t)$ at $t = t_c$. At $B_x = 1.95$ and $\Delta_c = -0.05$, $\lambda_c = -0.0013$. We choose this ramping rate because it reflects the dynamics of the cavity-coupled model near the critical point, where the breaking of the adiabaticity occurs. The ground state probability P_g of this linearly-ramped model [Fig. 2(b)] shows similar behavior as the cavity-coupled TFIM. The final probability is $P_g(T) = 0.967$, with only 1% deviation from that of the cavity-coupled model. The onset of the probability decrease occurs earlier in this case, as $B_x(t)$ reaches the critical point at an earlier time than $\tilde{B}_x(t)$. With this model, we can also estimate the quasiparticle excitations using the Landau-Zener formula [50, 51]. As shown in [52, 53], the excitation probability of the $(k, -k)$ pair is

$$P_k^{(LZ)} = \exp(-2\pi J_0^2 k^2 / \lambda_c). \quad (7)$$

The ground state probability is $P_g^{(LZ)} = \prod_k (1 - P_k^{(LZ)})$. With our parameters, $P_g^{(LZ)} = 0.966$, very close to the results from the numerical simulations. As shown in Fig. 2(c) and (d), this formula gives accurate estimation in a large range of parameters. The study of this linearly-ramped model thus reveals that the quench dynamics of the cavity-coupled TFIM is due to the cavity-induced nonlinearity combined with the breaking of the adiabaticity near the critical point.

Dynamics during slow ramping.—Another interesting case is when the driving field is gradually ramped through the bistable regime with the initial and the final states of the TFIM in different phases. Assume that the driving field is $\epsilon(t) = \epsilon_0 + (\epsilon_f - \epsilon_0)t/T$ for time $0 < t \leq T$ and $\epsilon(t) = \epsilon_f$ for $T < t \leq 1.2T$, where ϵ_0 (ϵ_f) is the initial (final) driving and T ($1.2T$) is the duration of the ramping (entire evolution). Here the driving is first

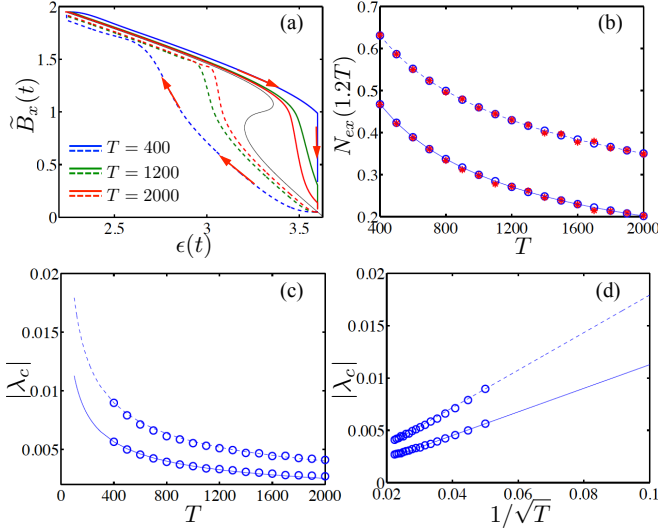


FIG. 3. (Color online) (a) The effective transverse field \tilde{B}_x vs. ϵ during slow ramping. Solid (dashed) lines: ramping up (down) at $T = 400, 1200, 2000$ from top to bottom (bottom to top); thin solid line: stationary solution. (b) N_{ex} at $t = 1.2T$ vs. T . Blue circles and solid (dashed) line: cavity-coupled TFIM, ramping up (down); red stars: Landau-Zener formula. (c) and (d) $|\lambda_c|$ vs. T and $1/\sqrt{T}$. Blue circles: simulation; solid (dashed) lines: $20|\lambda_c(T = 400)|/\sqrt{T}$ when ramping up (down). The parameters are the same as that in Fig. 1(b).

slowly ramped to ϵ_f , and then parked at ϵ_f for a duration of $0.2T$ to let the system relax towards the stationary state. Let $\epsilon_0 = 2.23$, corresponding to an initial transverse field $\tilde{B}_x(0) = 1.95$ [$x_a^{(s)} = 0$] with our parameters; and $\epsilon_f = 3.6$, which gives $\tilde{B}_x \approx 0.05$ in the stationary state. We study the dynamical phase transition during the ramping numerically [3]. Fig. 3(a) shows the correspondence between the transverse field $\tilde{B}_x(t)$ and the driving $\epsilon(t)$ during the evolution. For the shortest ramping time $T = 400$, \tilde{B}_x decreases barely below the critical point by the end of the ramping at $t = T$ and continues to decrease during the parking time $T < t \leq 1.2T$, which produces a large vertical segment in the plot. For the longest time $T = 2000$, \tilde{B}_x almost reaches its stationary value by $t = T$ with only a small decrease during the parking time. In all evolutions, different from the stationary solution, the TFIM remains in the paramagnetic phase when the driving reaches the bifurcation point ϵ_2 ; and enters the ferromagnetic phase at a later time. A hysteresis loop that encloses the stationary solution appears when the driving is first ramped up to ϵ_f and then back down to ϵ_0 [49]. For shorter ramping time, the loop is farther away from the stationary result. This is due to the finite relaxation time of the cavity-coupled model at a given cavity damping rate. In particular, large deviations from the stationary solution appear near the bifurcation points where system parameters evolve fast.

During the ramping, quasiparticles are created when

the effective transverse field is at the vicinity of the critical point. In Fig. 3(b), we plot the number of quasiparticle pairs $N_{ex} = \sum_{k>0} |\beta_k|^2$ at the final time $t = 1.2T$, calculated from the probability amplitude β_k of the excited state, as a function of the ramping time T . It is shown that the excitation number decreases quickly with T . For comparison, we use the Landau-Zener formula to estimate the excitation in a linearly-ramped TFIM with a ramping rate λ_c defined above. As shown in Fig. 3(b), the estimation agrees well with the numerical result of the cavity-coupled TFIM, with a maximum deviation of only 0.007. The ramping rate λ_c is thus a crucial factor to characterize the adiabaticity of the time evolution of the cavity-coupled model. In Fig. 3(c) and (d), $|\lambda_c|$ is plotted versus the ramping time T and $1/\sqrt{T}$, respectively. We find that the dependence of λ_c on T can be approximated by the expression $\lambda_c \approx 20\lambda_c(T=400)/\sqrt{T}$ with a maximum discrepancy of 3.6% $|\lambda_c|$. This inverse-square-root dependence of λ_c on T is caused by the nonlinearity in the cavity-coupled model. Our result indicates that by controlling the cavity-induced nonlinearity, the adiabaticity of this dynamical process can be adjusted.

Discussions.—The cavity-coupled TFIM can be realized with superconducting systems. It was shown that superconducting qubits, such as flux qubit and transmon, can be connected in an array to form the one-dimensional TFIM [29, 40–44]. The qubits can then be coupled to a superconducting resonator that acts as the cavity. Moreover, the effects studied here can be demonstrated using a finite-sized TFIM with only a few qubits. In our analysis, we neglect the decoherence of the qubits, which could cause the quasiparticles in the TFIM to decay. In order to reliably characterize the dynamical quantum phase transition and the scaling of the quasiparticle creation, it is required that the duration of the time evolution be much shorter than the decay time. In superconducting qubits, decoherence time on the order of $100\mu s$ has been observed in experiments [2]. For a coupling strength of $J_0/2\pi = 1\text{GHz}$, a duration of $T = 2000$ used in our simulation corresponds to 318 ns., much shorter than the decoherence time of the qubits.

In treating the interaction between the qubits and the resonator, we use a mean-field approach to decompose the total Hamiltonian into separate parts for the TFIM and for the cavity. This approach is valid for cavity fields under strong driving [46]. With our parameters, the cavity field can be viewed as a coherent state with amplitude $\langle \hat{a} \rangle \sim 50$ and photon number $N_a \sim 2500$. The ratio of the quantum fluctuations with respect to the cavity photon number is then $1/\sqrt{N_a} \sim 0.02 \ll 1$ and the fluctuations can be neglected.

Conclusions.—To conclude, we study the quench dynamics near the bifurcation points of a quantum many-body system coupled to a cavity. The coupling between the many-body model and the cavity induces nonlinearity and a bistable regime in the phase diagram. The time

evolutions of this system after a sudden quench at the bifurcation points and during a slow ramping of the cavity driving are simulated numerically. Our results show that the cavity-induced nonlinearity plays an essential role in the dynamical quantum phase transition of the cavity-coupled system, and it can strongly affect the adiabaticity of the time evolution. This study indicates that the adiabaticity and fidelity of adiabatic quantum processes could be improved by controlling such nonlinearity.

Acknowledgements. This work is supported by the National Science Foundation under Award # 0956064. The author thanks the Institute of Physics, Chinese Academy of Sciences, for hospitality.

* ltian@ucmerced.edu

- [1] T. Langen, R. Geiger, and J. Schmiedmayer, *Annu. Rev. Condens. Matter Phys.* **6**, 201 (2015).
- [2] M. H. Devoret and R. J. Schoelkopf, *Science* **339**, 1169 (2013).
- [3] J. Dziarmaga, *Adv. Phys.* **59**, 1063 (2010).
- [4] A. Polkovnikov, K. Sengupta, A. Silva, and M. Vengalattore, *Rev. Mod. Phys.* **83**, 863 (2011).
- [5] A. del Campo and W. H. Zurek, *Int. J. Mod. Phys. A* **29**, 1430018 (2014).
- [6] J. Eisert, M. Friesdorf, and C. Gogolin, *Nat. Phys.* **11**, 124 (2015).
- [7] W. H. Zurek, U. Dorner, and P. Zoller, *Phys. Rev. Lett.* **95**, 105701 (2005).
- [8] A. Polkovnikov, *Phys. Rev. B* **72**, 161201 (2005).
- [9] T. W. B. Kibble, *J. Phys. A* **9**, 1387 (1976).
- [10] W. H. Zurek, *Nature (London)* **317**, 505 (1985).
- [11] W. H. Zurek, *Phys. Rep.* **276**, 177 (1996).
- [12] T. Kibble, *Phys. Today* **60**, 47 (2007).
- [13] R. Barankov and A. Polkovnikov, *Phys. Rev. Lett.* **101**, 076801 (2008).
- [14] D. Sen, K. Sengupta, and S. Mondal, *Phys. Rev. Lett.* **101**, 016806 (2008).
- [15] A. Chandran, A. Erez, S. S. Gubser, and S. L. Sondhi, *Phys. Rev. B* **86**, 064304 (2012).
- [16] T. Caneva, M. Murphy, T. Calarco, R. Fazio, S. Montangero, V. Giovannetti, and G. E. Santoro, *Phys. Rev. Lett.* **103**, 240501 (2009).
- [17] A. del Campo, M. M. Rams, and W. H. Zurek, *Phys. Rev. Lett.* **109**, 115703 (2012).
- [18] B. Damski, *J. Stat. Mech.* **2014**, P12019 (2014).
- [19] S. Deffner, C. Jarzynski, and A. del Campo, *Phys. Rev. X* **4**, 021013 (2014).
- [20] A. T. Rezakhani, W.-J. Kuo, A. Hamma, D. A. Lidar, and P. Zanardi, *Phys. Rev. Lett.* **103**, 080502 (2009).
- [21] J. M. Raimond, M. Brune, and S. Haroche, *Rev. Mod. Phys.* **73**, 565 (2001).
- [22] S. M. Girvin, in *Lecture Notes on Strong Light-Matter Coupling: from Atoms to Solid-State Systems* (World Scientific, Singapore, 2013).
- [23] J. Q. You and F. Nori, *Nature (London)* **474**, 589 (2011).
- [24] H. Ritsch, P. Domokos, F. Brennecke, and T. Esslinger, *Rev. Mod. Phys.* **85**, 553 (2013).
- [25] C. Emary and T. Brandes, *Phys. Rev. E* **67**, 066203 (2003).
- [26] C. Maschler and H. Ritsch, *Phys. Rev. Lett.* **95**, 260401 (2005).
- [27] J. Larson, B. Damski, G. Morigi, and M. Lewenstein, *Phys. Rev. Lett.* **100**, 050401 (2008).
- [28] W. Chen, K. Zhang, D. S. Goldbaum, M. Bhattacharya, and P. Meystre, *Phys. Rev. A* **80**, 011801(R) (2009).
- [29] L. Tian, *Phys. Rev. Lett.* **105**, 167001 (2010).
- [30] J. M. Fink, R. Bianchetti, M. Baur, M. Göppl, L. Steffen, S. Filipp, P. J. Leek, A. Blais, and A. Wallraff, *Phys. Rev. Lett.* **103**, 083601 (2009).
- [31] P. Macha, G. Oelsner, J.-M. Reiner, M. Marthaler, S. André, G. Schön, U. Huebner, H.-G. Meyer, E. Ilichev, and A. V. Ustinov, *Nat. Commun.* **5**, 5146 (2014).
- [32] J. Klinder, H. Keßler, M. Wolke, L. Mathey, and A. Hemmerich, *Proc. Natl. Acad. Sci.* **112**, 3290 (2015).
- [33] A. A. Houck, H. E. Türeci, and J. Koch, *Nat. Phys.* **8**, 292 (2012).
- [34] K. Seo and L. Tian, *Phys. Rev. B* **91**, 195439 (2015).
- [35] S. Sachdev, *Quantum Phase Transitions* (Cambridge University Press, Cambridge, England, 1999).
- [36] J. Dziarmaga, *Phys. Rev. Lett.* **95**, 245701 (2005).
- [37] E. Farhi, J. Goldstone, S. Gutmann, J. Lapan, A. Lundgren, and D. Preda, *Science* **292**, 472 (2001).
- [38] G. E. Santoro, R. Martonák, E. Tosatti, and R. Car, *Science* **295**, 2427 (2002).
- [39] S. Boixo, T. F. Rønnow, S. V. Isakov, Z. Wang, D. Wecker, D. A. Lidar, J. M. Martinis, and M. s Troyer, *Nat. Phys.* **10**, 218 (2014).
- [40] L. S. Levitov, T. P. Orlando, J. B. Majer, and J. E. Mooij, eprint [arXiv:cond-mat/0108266](https://arxiv.org/abs/cond-mat/0108266).
- [41] Y.-D. Wang, F. Xue, Z. Song, and C.-P. Sun, *Phys. Rev. B* **76**, 174519 (2007).
- [42] O. Viehmann, J. von Delft, and F. Marquardt, *Phys. Rev. Lett.* **110**, 030601 (2013).
- [43] H. You, M. R. Geller, and P. C. Stancil, *Phys. Rev. A* **87**, 032341 (2013).
- [44] L. H. Du, J. Q. You, and L. Tian, *Phys. Rev. A* **92**, 012330 (2015).
- [45] See the Supplemental Materials for detailed derivations.
- [46] T. Mori, *J. Stat. Mech. Theo. Exp.* **2013**, P06005 (2013).
- [47] D. F. Walls and G. J. Milburn, *Quantum Optics* (Springer, Berlin, Heidelberg, 2008).
- [48] E. X. DeJesus and C. Kaufman, *Phys. Rev. A* **35**, 5288 (1987).
- [49] P. G. Drazin, *Nonlinear Systems* (Cambridge University Press, Cambridge, England, 1992).
- [50] L. D. Landau, *Phys. Z. Sowjetunion* **2**, 46 (1932).
- [51] C. Zener, *Proc. R. Soc. London, Ser. A* **137**, 696 (1932).
- [52] B. Damski, *Phys. Rev. Lett.* **95**, 035701 (2005).
- [53] M. Gong, X. Wen, G. Sun, D.-W. Zhang, Y. Yu, S.-L. Zhu, S. Han, eprint [arXiv:1505.07362](https://arxiv.org/abs/1505.07362).

Supplementary Materials for “Cavity-assisted Dynamical Quantum Phase Transition at Bifurcation Points”

In this document, we present detailed results on the transverse field Ising model (TFIM) and the stability condition for a cavity coupled to a TFIM. These results are used in the main paper. In Sec. I, details on quasiparticle excitations, ground state properties, time-dependent wave function, and operator averages in a one-dimensional (1D) TFIM are presented. In Sec. II, derivations of the stationary solutions, stability condition, bifurcation points, and their dependence on the transverse field B_x and the detuning Δ_c are given.

I. PROPERTIES OF THE TRANSVERSE FIELD ISING MODEL

A. Quasiparticle excitations

The TFIM, also called the quantum Ising model, has been widely studied as a prototype for continuous quantum phase transition [S1]. Consider the Hamiltonian of a 1D TFIM ($\hbar = 1$)

$$H_s = -B_x \sum_i \hat{\sigma}_{xi} - J_0 \sum_i \hat{\sigma}_{zi} \hat{\sigma}_{z(i+1)}, \quad (S1)$$

where $\hat{\sigma}_{xi}$ and $\hat{\sigma}_{zi}$ are the Pauli matrices for the spin-1/2 particle at site i , B_x is a uniform transverse field, and J_0 is a ferromagnetic coupling between neighboring spins. We assume that the spin operators satisfy the periodic boundary condition: $\hat{\sigma}_{\alpha(N+1)} = \hat{\sigma}_{\alpha 1}$ with $\alpha = x, y, z$. This model is exactly solvable by applying the Jordan-Wigner transformation [S2]

$$\hat{\sigma}_{zi} = -(\hat{c}_i^\dagger + \hat{c}_i) \prod_{j=1}^{i-1} (1 - 2\hat{c}_j^\dagger \hat{c}_j), \quad \hat{\sigma}_{xi} = (1 - 2\hat{c}_i^\dagger \hat{c}_i), \quad (S2)$$

where \hat{c}_i (\hat{c}_i^\dagger) is the annihilation (creation) operator of a fermionic particle at site i . This transformation converts the quantum spins in the 1D TFIM to spineless fermions. In the fermionic representation, the Hamiltonian (S1) becomes

$$H_s = -J_0 \sum_i (\hat{c}_i^\dagger \hat{c}_{i+1}^\dagger + \hat{c}_i^\dagger \hat{c}_{i+1} + h.c.) + 2B_x \sum_i \hat{c}_i^\dagger \hat{c}_i - NB_x. \quad (S3)$$

Here the fermionic operators satisfy the anti-periodic boundary condition $\hat{c}_{N+1} = -\hat{c}_1$ in the subspace of zero or even number of excitations [S3]. Define the momentum space operators $\hat{c}_k = \sum_i e^{-ik_i} \hat{c}_i / \sqrt{N}$, where the wave vectors $k = \pm\pi(2m-1)/N$ with $1 \leq m \leq N/2$ are odd multiples of π/N under the anti-periodic boundary condition. In the momentum basis, the Hamiltonian then becomes

$$H_s = \sum_{k>0} \left[2(B_x - J_0 \cos k) (\hat{c}_k^\dagger \hat{c}_k + \hat{c}_{-k}^\dagger \hat{c}_{-k}) - 2iJ_0 \sin k (\hat{c}_k^\dagger \hat{c}_{-k}^\dagger - \hat{c}_{-k} \hat{c}_k) \right] - NB_x, \quad (S4)$$

where the k and $(-k)$ modes are coupled to each other.

The quasiparticle modes are defined using the Bogoliubov transformation

$$\hat{c}_k = u_k \hat{\gamma}_k + iv_k \hat{\gamma}_{-k}^\dagger, \quad (S5)$$

$$\hat{c}_{-k}^\dagger = iv_k \hat{\gamma}_k + u_k \hat{\gamma}_{-k}^\dagger, \quad (S6)$$

where $\hat{\gamma}_k$ ($\hat{\gamma}_k^\dagger$) is the annihilation (creation) operator of the k -momentum quasiparticle with the coefficients satisfying $u_{-k} = u_k$, $v_{-k} = -v_k$, and $u_k^2 + v_k^2 = 1$. The quasiparticle operators satisfy the commutation relations: $[\hat{\gamma}_k, \hat{\gamma}_l^\dagger]_+ = \delta_{kl}$ and $[\hat{\gamma}_k, \hat{\gamma}_l]_+ = 0$, where $[\hat{A}, \hat{B}]_+$ is the anti-commutator for operators \hat{A} and \hat{B} . It can also be shown that

$$\hat{\gamma}_k = u_k \hat{c}_k - iv_k \hat{c}_{-k}^\dagger, \quad (S7)$$

$$\hat{\gamma}_{-k}^\dagger = -iv_k \hat{c}_k + u_k \hat{c}_{-k}^\dagger. \quad (S8)$$

Let the coefficients be $u_k = \cos \theta_k$ and $v_k = \sin \theta_k$ with

$$\sin(2\theta_k) = \frac{J_0 \sin k}{\sqrt{J_0^2 + B_x^2 - 2B_x J_0 \cos k}}, \quad \cos(2\theta_k) = \frac{B_x - J_0 \cos k}{\sqrt{J_0^2 + B_x^2 - 2B_x J_0 \cos k}}. \quad (S9)$$

The Hamiltonian (S4) can then be written in terms of the quasiparticle modes as

$$H_s = \sum_k \varepsilon_k \hat{\gamma}_k^\dagger \hat{\gamma}_k + E_g, \quad (\text{S10})$$

where the summation is over all wave vectors (both $k \geq 0$ and $k < 0$). The eigenenergy of the quasiparticle $\hat{\gamma}_k$ is

$$\varepsilon_k = 2\sqrt{J_0^2 + B_x^2 - 2B_x J_0 \cos k} \quad (\text{S11})$$

with $\varepsilon_k = \varepsilon_{-k}$. At the quantum critical point with $B_x = J_0$, $\varepsilon_k = 4J_0|\sin(k/2)|$, which approaches zero as $k \rightarrow 0$. The ground state energy is $E_g = \sum_{k>0} \varepsilon_k [\cos(2\theta_k) - 1]$. Equation (S10) shows that the TFIM is an integrable model, where quasiparticles in different $(k, -k)$ basis are not coupled.

B. Ground state properties

The ground state of the TFIM satisfies $H_s|G\rangle = E_g|G\rangle$. For an arbitrary momentum k , we have $\hat{\gamma}_k|G\rangle = 0$. In the most general form, the ground state can be written as

$$|G\rangle = \prod_{k>0} (a_k + b_k \hat{c}_k^\dagger + b_{-k} \hat{c}_{-k}^\dagger + d_k \hat{c}_k^\dagger \hat{c}_{-k}^\dagger) |0_{k,-k}\rangle, \quad (\text{S12})$$

which contains a superposition of all possible states in each $(k, -k)$ subspace. Here $|0_{k,-k}\rangle$ is the vacuum state of the $(k, -k)$ modes. Using the conditions $\hat{\gamma}_k|G\rangle = 0$ and $\hat{\gamma}_{-k}|G\rangle = 0$, we find that

$$b_k = 0, \quad b_{-k} = 0, \quad d_k u_k = i v_k a_k. \quad (\text{S13})$$

Combining these results with the normalization condition, the ground state wave function can be written as $|G\rangle = \prod_{k>0} |G_k\rangle$ with

$$|G_k\rangle = \left(u_k + i v_k \hat{c}_k^\dagger \hat{c}_{-k}^\dagger \right) |0_{k,-k}\rangle \quad (\text{S14})$$

being the ground state in the $(k, -k)$ subspace. It can also be shown that

$$\hat{\gamma}_k^\dagger |G_k\rangle = \hat{c}_k^\dagger |0_{k,-k}\rangle, \quad \hat{\gamma}_{-k}^\dagger |G_k\rangle = \hat{c}_{-k}^\dagger |0_{k,-k}\rangle, \quad (\text{S15})$$

which tell us that the creation of one quasiparticle $\hat{\gamma}_{\pm k}$ in the ground state $|G_k\rangle$ corresponds to the generation of one physical particle $\hat{c}_{\pm k}$ in the vacuum state. Furthermore,

$$i \hat{\gamma}_k^\dagger \hat{\gamma}_{-k}^\dagger |G_k\rangle = \left(-v_k + i u_k \hat{c}_k^\dagger \hat{c}_{-k}^\dagger \right) |0_{k,-k}\rangle, \quad (\text{S16})$$

which contains two quasiparticles, one in the $\hat{\gamma}_k$ mode and the other in the $\hat{\gamma}_{-k}$ mode. This state is orthogonal to the ground state $|G_k\rangle$ in the $(k, -k)$ subspace.

C. Time-dependent wave function

The Hamiltonian (S4) (and similarly, \tilde{H}_s under an effective transverse field \tilde{B}_x as discussed in the main paper) only contains the following terms: $\hat{c}_k^\dagger \hat{c}_k$, $\hat{c}_k^\dagger \hat{c}_{-k}^\dagger$ and $\hat{c}_{-k} \hat{c}_k$. These terms conserve the parity of a quantum state during a time evolution, i.e., the number of fermionic particles will remain in the even (or odd) subspace during the entire evolution. Hence starting from an initial state with even (odd) number of fermionic particles, the TFIM governed by a time-dependent Hamiltonian will always have even (odd) number of particles during the evolution. In particular, starting from the ground state of an initial transverse field, the number of fermionic particles or quasiparticles will always be an even number as the transverse field varies with time. The wave function at an arbitrary time t can then be written as $|\psi(t)\rangle = \prod_{k>0} (U_k(t) + i V_k(t) \hat{c}_k^\dagger \hat{c}_{-k}^\dagger) |0\rangle$ with time-dependent coefficients $U_k(t)$ and $V_k(t)$.

Assume that the instantaneous Hamiltonian at time t is $H_s(t)$ with the instantaneous ground state $|G(t)\rangle = \prod_{k>0} |G_k(t)\rangle$. The above wave function can be decomposed as

$$|\psi(t)\rangle = \prod_{k>0} [\alpha_k(t) + i \beta_k(t) \hat{\gamma}_k^\dagger \hat{\gamma}_{-k}^\dagger] |G_k(t)\rangle, \quad (\text{S17})$$

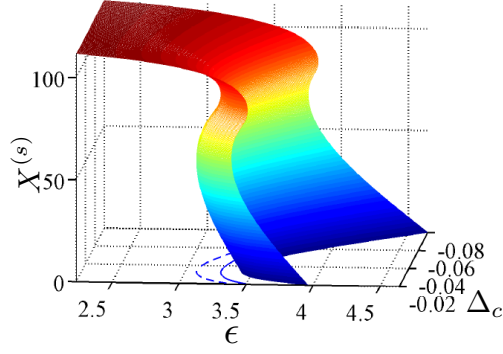


FIG. S1. (Color online) The operator average $X^{(s)}$ vs. driving amplitude ϵ and detuning Δ_c . Solid (dashed) line: the bifurcation point ϵ_2 (ϵ_1) vs. Δ_c . The parameters are $J_0 = 1$, $B_x = 1.95$, $g = 0.02$ and $\kappa = 0.07$, all in arbitrary units; and the TFIM has $N = 120$ sites

where $\hat{\gamma}_k$ is the annihilation operator of the instantaneous quasiparticle mode. The probability amplitudes can be derived as $\alpha_k(t) = [u_k, v_k] \cdot [U_k(t), V_k(t)]^T$ and $\beta_k(t) = [-v_k, u_k] \cdot [U_k(t), V_k(t)]^T$ with “T” being the transpose operation. The wave function in the $(k, -k)$ subspace is then a superposition of the ground state $|G_k(t)\rangle$ with probability amplitude $\alpha_k(t)$ and the excited state $i\hat{\gamma}_k^\dagger \hat{\gamma}_{-k}^\dagger |G_k(t)\rangle$ with probability amplitude $\beta_k(t)$.

D. Operator average of $\sum_i \hat{\sigma}_{xi}$

When the wave function is known, the properties of the TFIM can be studied by calculating various operator averages. For example, the equal-time correlation function $C_{ij} = \langle G | \hat{\sigma}_{zi} \hat{\sigma}_{zj} | G \rangle$ between the operators $\hat{\sigma}_{zi}$ and $\hat{\sigma}_{zj}$ can be used to characterize the quantum phase transition in the TFIM. In our system, the cavity field is coupled to the TFIM via the operator $\sum_i \hat{\sigma}_{xi}$. The average of this operator plays an important role in the dynamics of the cavity-coupled system.

In the representation of the fermionic modes,

$$\sum_i \hat{\sigma}_{xi} = N - 2 \sum_k \hat{c}_k^\dagger \hat{c}_k. \quad (\text{S18})$$

For an arbitrary state $|\psi(t)\rangle = \prod_{k>0} (U_k + iV_k \hat{c}_k^\dagger \hat{c}_{-k}^\dagger) |0\rangle$, we derive the operator average of $\sum_i \hat{\sigma}_{xi}$ as

$$X = \left\langle \psi(t) \left| \sum_i \hat{\sigma}_{xi} \right| \psi(t) \right\rangle = N - 4 \sum_{k>0} |V_k|^2, \quad (\text{S19})$$

which is determined by the coefficients $\{V_k\}$. For the ground state $|G\rangle$ of a large lattice ($N \rightarrow \infty$), we find that

$$X = \frac{N}{2\pi} \int_{-\pi}^{\pi} dk \frac{B_x - J_0 \cos k}{\sqrt{J_0^2 + B_x^2 - 2B_x J_0 \cos k}}. \quad (\text{S20})$$

In the limiting case of $B_x \gg J_0$, $\langle G | \sum_i \hat{\sigma}_{xi} | G \rangle \rightarrow N$; and at $B_x \ll J_0$, $\langle G | \sum_i \hat{\sigma}_{xi} | G \rangle \rightarrow 0$.

II. BIFURCATION AND STABILITY CONDITION

A. Stationary solutions

As discussed in the main paper, the Langevin equation for the average of the cavity annihilation operator is [S4]

$$\frac{d}{dt} \langle \hat{a} \rangle = i\Delta_c \langle \hat{a} \rangle - \frac{\kappa}{2} \langle \hat{a} \rangle + i(\epsilon - gX), \quad (\text{S21})$$

where $\Delta_c = \omega_d - \omega_c$ is the cavity detuning with respect to the driving frequency ω_d , ω_c is the frequency of the cavity mode, κ is the cavity damping rate, ϵ is the driving amplitude, and g is the coupling strength between the spins and the cavity as denoted in the main paper. The conjugate equation of (S21) is

$$\frac{d}{dt} \langle \hat{a}^\dagger \rangle = -i\Delta_c \langle \hat{a}^\dagger \rangle - \frac{\kappa}{2} \langle \hat{a}^\dagger \rangle - i(\epsilon - gX), \quad (\text{S22})$$

where we have assumed that the driving amplitude is a real number for simplicity of discussion. Let $x_a = \langle (\hat{a} + \hat{a}^\dagger) \rangle$ and $p_a = -i\langle (\hat{a} - \hat{a}^\dagger) \rangle$ be the averages of the coordinate and momentum quadratures of the cavity field, respectively. From Eqns. (S21) and (S22), we obtain

$$\frac{d}{dt} x_a = -\Delta_c p_a - \frac{\kappa}{2} x_a, \quad (\text{S23})$$

$$\frac{d}{dt} p_a = \Delta_c x_a - \frac{\kappa}{2} p_a + 2(\epsilon - gX), \quad (\text{S24})$$

which depend on the state of the TFIM through the gX term. The stationary solutions satisfy the relations $dx_a/dt = 0$ and $dp_a/dt = 0$. Meanwhile, $X^{(s)} = \langle G | \sum_i \hat{\sigma}_{xi} | G \rangle$, where $|G\rangle$ is the ground state of the TFIM under the effective transverse field $\tilde{B}_x = B_x - gx_a^{(s)}$. The operator average $X^{(s)}$ is then a nonlinear function of the stationary cavity displacement $x_a^{(s)}$. Hence, we obtain

$$x_a^{(s)} = \frac{2\Delta_c [-\epsilon + gX^{(s)}]}{\Delta_c^2 + \kappa^2/4}, \quad (\text{S25})$$

$$p_a^{(s)} = -(\kappa/2\Delta_c) x_a^{(s)}. \quad (\text{S26})$$

Because of the nonlinear dependence of $X^{(s)}$ on $x_a^{(s)}$, the coupled system has a bistable regime, where there exist three stationary solutions at a given driving amplitude ϵ . One of these solutions corresponds to $\tilde{B}_x > 1$ with the TFIM in the paramagnetic phase, another solution has $\tilde{B}_x < 1$ in the ferromagnetic phase, and the third solution has an intermediate value in-between these two. The dependence of the stationary cavity displacement $x_a^{(s)}$ on the driving amplitude ϵ and detuning Δ_c has been presented in the main paper. For the TFIM, the effective field \tilde{B}_x is directly related to $x_a^{(s)}$, and so does the operator average $X^{(s)}$. In Fig. S1, we plot $X^{(s)}$ as a function of ϵ and Δ_c , which clearly demonstrates the bistability of the cavity-coupled TFIM. The bifurcation points are also plotted in this figure as the solid and the dashed lines.

B. Stability condition

Here we study the stability of the above stationary solutions. Assume that the cavity has a small offset \tilde{x}_a (\tilde{p}_a) from its stationary value in the coordinate (momentum) quadrature, i.e., $x_a = x_a^{(s)} + \tilde{x}_a$ ($p_a = p_a^{(s)} + \tilde{p}_a$). We linearize the operator average as

$$X = X^{(s)}(x_a^{(s)}) + X' \cdot \tilde{x}_a \quad (\text{S27})$$

with the derivative $X' = dX^{(s)}/dx_a^{(s)}$. Using Eqns. (S23, S24, S27), we obtain

$$\frac{d}{dt} \begin{bmatrix} \tilde{x}_a \\ \tilde{p}_a \end{bmatrix} = \begin{bmatrix} -\kappa/2 & -\Delta_c \\ \Delta_c - 2gX' & -\kappa/2 \end{bmatrix} \begin{bmatrix} \tilde{x}_a \\ \tilde{p}_a \end{bmatrix}, \quad (\text{S28})$$

which are dynamic equations for the small offsets. Let the eigensolution of the coupled equations in (S28) have the form $e^{\lambda t}$. The secular frequencies can be derived as

$$\lambda_{\pm} = -\frac{\kappa}{2} \pm \sqrt{(2\Delta_c gX' - \Delta_c^2)}. \quad (\text{S29})$$

When the real part of one of the secular frequencies is positive, the stationary solution becomes unstable [S5]. For $\Delta_c < 0$, the stability condition of this system can then be derived as

$$\frac{\Delta_c^2 + \kappa^2/4}{2\Delta_c} < gX'. \quad (\text{S30})$$

An interesting property of the stability condition is its connection to the derivative of the driving amplitude ϵ with respect to the stationary cavity displacement $x_a^{(s)}$. By conducting a differentiation with respect to $x_a^{(s)}$ on both sides of Eq. (S25), we have

$$\frac{d\epsilon}{dx_a^{(s)}} = gX' - \frac{\Delta_c^2 + \kappa^2/4}{2\Delta_c}. \quad (\text{S31})$$

Hence, the stability of a stationary solution (S30) is equivalent to the positivity of its slope, i.e., $d\epsilon/dx_a^{(s)} > 0$. Among the three solutions at a given driving amplitude, the smallest solution and the largest solution are both stable with positive slopes. The smallest (largest) solution corresponds to the TFIM in the paramagnetic (ferromagnetic) phase. The intermediate solution is unstable with a negative slope $d\epsilon/dx_a^{(s)} < 0$. Outside the bistable regime, the system has only one stable solution at a given ϵ , as shown in Fig.1 of the main paper.

C. Bifurcation points

When passing across the bifurcation points, the system switches between the bistable regime and regimes with only one stationary solution. Moreover, the TFIM makes a switching from the paramagnetic phase to the ferromagnetic phase, or vice versa. In the cavity-coupled model, the bifurcation points satisfy the condition

$$d\epsilon/dx_a^{(s)} = 0. \quad (\text{S32})$$

With Eq. (S31), this condition can be expressed as

$$gX' = \frac{\Delta_c^2 + \kappa^2/4}{2\Delta_c}. \quad (\text{S33})$$

From Eq. (S33), it is interesting to note that X' at the bifurcation points does not depend on the original transverse field B_x in the TFIM. This observation indicates that the effective transverse field \tilde{B}_x at the bifurcation points, as well as the operator average $X^{(s)}$, does not depend on B_x . Because $\tilde{B}_x = B_x - gx_a^{(s)}$, the stationary cavity displacement $x_a^{(s)}$ at the bifurcation points thus has a linear dependence on the original transverse field B_x . Combining these results with Eq. (S25), we find that the driving amplitude at the bifurcation points ($\epsilon_{1,2}$) also has a linear dependence on B_x at given values of Δ_c , κ , and g . This can be seen in Fig. S2(a), where $\epsilon_{1,2}$ are plotted as functions of B_x with all other parameters fixed. As \tilde{B}_x is independent of B_x , the state of the TFIM at the bifurcation points is also independent of B_x . Subsequently, the dynamics of the TFIM after a sudden quench at the bifurcation points does not depend on B_x either. This is proven by our numeral simulation of the time evolution of the cavity-coupled TFIM at different values of B_x . As shown in Fig.2(c) of the main paper, the ground state probability $P_g(T)$ at the final time T is almost independent of B_x , with only small variations caused by numerical inaccuracies.

In contrast, X' at the bifurcation points depends on the detuning Δ_c . Hence the bifurcation points $\epsilon_{1,2}$ show more complicated dependence on Δ_c than on B_x , as shown in Fig. S2(b), where $\epsilon_{1,2}$ are plotted as functions of the detuning Δ_c . Hence the effective transverse field \tilde{B}_x at $\epsilon_{1,2}$ varies with the detuning, which affects the dynamics and the quasiparticle excitations during the switching process. The ground state probability versus the detuning is plotted in Fig.2(d) of the main paper.

* ltian@ucmerced.edu

- [S1] S. Sachdev, *Quantum Phase Transitions* (Cambridge University Press, Cambridge, England, 1999).
- [S2] P. Jordan and E. Wigner, Z. Phys. **47**, 631 (1928).
- [S3] J. Dziarmaga, Phys. Rev. Lett. **95**, 245701 (2005).
- [S4] D. F. Walls and G. J. Milburn, *Quantum Optics* (Springer, Berlin, Heidelberg, 2008).
- [S5] E. X. DeJesus and C. Kaufman, Phys. Rev. A **35**, 5288 (1987).

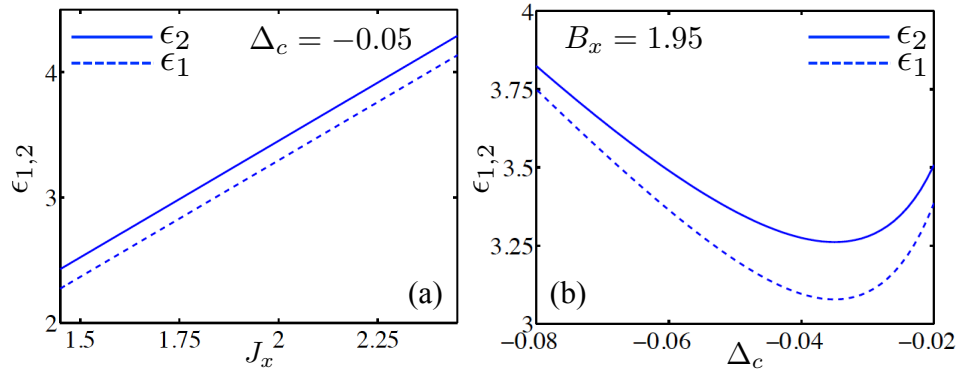


FIG. S2. (Color online) (a) The bifurcation points $\epsilon_{1,2}$ vs. B_x at a given detuning. (b) The bifurcation points $\epsilon_{1,2}$ vs. Δ_c at a given transverse field. Solid lines: ϵ_2 ; dashed lines: ϵ_1 . The parameters are the same as that in Fig. S1.